ELSEVIER

Ecological Modelling 144 (2001) 295–314

ECOLOGICAL MODELLING

www.elsevier.com/locate/ecolmodel

Simulations of phytoplankton seasonal cycle with multi-level and multi-layer physical-ecosystem models: the Black Sea example

Temel Oguz [a,*], Paola Malanotte-Rizzoli [b], Hugh W. Ducklow [c]

[a] *Institute of Marine Sciences, Middle East Technical University, PO Box 28, Erdemli, 33731, Icel, Turkey*
[b] *Department of Earth, Atmospheric and Planetary Sciences, Massachusettes Institute of Technology, Cambridge, MA 02139, USA*
[c] *Virginia Institute of Marine Sciences, The College of William and Mary, Gloucester Point, VA, USA*

Received 27 July 2000; received in revised form 20 March 2001; accepted 22 May 2001

Abstract

Using the Black Sea ecosystem as an example, the phytoplankton seasonal cycle is simulated by several coupled physical-ecosystem models with different vertical resolutions, but the same biological setting. First, a high resolution multi-level model having a vertical grid spacing of about 3 m is shown to reproduce the observed annual phytoplankton structure reasonably well. This simulation is then compared with its multi-layer alternatives to investigate feasibility of using a relatively simpler model, and to look for its optimum vertical configuration. The simplest model involving a three layer structure provides only general features of the multi-level model simulation. It is able to reproduce the autumn and spring blooms taking place in the mixed layer, but it is not equally successful for simulating the summer production within the intermediate layer below the seasonal thermocline. It is found that this deficiency of the model is related to its poor nutrient recycling capability. Resolving the intermediate layer in the form of two sub-layers (i.e. increasing the model resolution to the four layer case) is shown to improve the efficiency of nutrient recycling and lead to a much better agreement of the results with those of its multi-level model. Further resolution introduced into the mixed layer, however, does not improve the performance of the layer models further. The key conclusion from our analysis is that, despite simplicity of its vertical configuration, the four layer model emerges as a practical alternative tool to its more complex, and computationally more demanding multi-level counterpart, particularly for three dimensional applications. Moreover, the Kraus–Turner type bulk surface-layer dynamics implemented in the multi-layer models are shown to be very efficient in simulating observed mixed layer characteristics as well as those deduced from the more sophisticated Mellor–Yamada level 2.5 turbulence closure parameterization of the multi-level model.

Keywords: Ecosystem modelling; Mixed-layer dynamics; Multi-layer model; Multi-level model; Phytoplankton productivity; Nutrient cycling; Black Sea

* Corresponding author. Tel.: +90-324-521-2150; fax: +90-324-521-2327.
E-mail address: oguz@ims.metu.edu.tr (T. Oguz).

0304-3800/01/$ - see front matter
PII: S0304-3800(01)00378-7

1. Introduction

Even though mixed layer depth variations and vertical mixing have been recognized as two primary factors controlling marine biological production for half a century (Sverdrup, 1953), the role of upper ocean physics on biogeochemical models has been explicitly incorporated only recently, after mid-1990s, through the development of coupled, vertically-resolved, physical circulation/plankton dynamics models involving sophisticated turbulence parameterizations. Earlier marine ecosystem models generally involved a zero-dimensional (i.e. vertically-homogeneous, single layer) structure assuming it as the sole biologically active part of the water column. This layer represented either the mixed layer or the euphotic zone; the choice was made depending on the particular problem under consideration (e.g. Pace et al., 1984; Evans and Parslow, 1985; Franks et al., 1986; Fasham et al., 1990; Taylor et al., 1993; Lebedeva and Shushkina, 1994; Hurtt and Armstrong, 1996; Lancelot et al., 2000). These models incorporated details of upper ocean physics, namely mixed layer depth variations and associated changes in the entrainment rate, directly from observations. However, unless there exits detailed time series measurements resolving daily-to-weekly variations, this approach becomes rather ambiguous because the results of such models depend critically on temporal variations of the mixed layer depth, especially during the winter-to-spring transition period (Eigenheer et al., 1996).

Various observations (e.g. Towsend et al., 1992; Stramska and Dickey, 1993) and model simulations (e.g. Stramska and Dickey, 1994; Oguz et al., 1996) suggested that the spring bloom can take place within the upper part of the deep mixed layer as soon as the convection weakens and the water column gains a slight stability, prior to mixed layer shallowing. The zero-dimensional models, on the other hand, tend to provide a delayed springtime response of the phytoplankton until vernal warming causes abrupt shallowing of the mixed layer depth, when the mixed layer-average photosynthetically available irradiance can trigger primary production. They also underestimate the summer biological production because they exclude all trophodynamic interactions at depths below the seasonal thermocline. When considering the euphotic zone instead of the mixed layer, the average irradiance over a relatively deep layer leads to somewhat weaker summer production. Features like the subsurface chlorophyll maximum are smeared out due to the depth averaging.

Two possible approaches to improve the performance of the zero-dimensional models are description of water column biogeochemical structure either at a series of vertical levels (multi-level approach) or layers (multi-layer approach). Multi-level models solve the equations at a sequence of computational levels separated from each other by a distance of the order of 5 m, and, therefore, reveal rather continuous variations of all state variables in the vertical (Jamart et al., 1977; Aknes and Lie, 1990; Varela et al., 1992; Doney et al., 1996; McClain et al., 1996; Levy et al., 1998; Gregoire et al., 1998; Oschlies and Garcon, 1999). Multi-layer models, on the other hand, approximate the same structure as a series of successive, interactive layers; each of which possesses vertically uniform properties (Rass et al., 1993; Taylor and Stephens, 1993; Dadou et al., 1996; McCreary et al., 1996; Anderson and Williams, 1998; Oguz and Salihoglu, 2000). Ideally, as the number of layers is increased, solution of a multi-layer model tends to approach to that given by a multi-level model. However, multi-layer models are developed to obtain reasonably realistic, but computationally more efficient solutions of three-dimensional problems by representing the vertical biogeochemical structure in the form of several layers (most often, three layers). Under such conditions, the multi-layer models may offer an effective alternative tool to their computationally more demanding multi-level counterparts.

Coupling of an ecosystem model with an upper ocean physical model allows a description of the mixed layer characteristics through a set of equations and the meteorological data with a tolerable degree of realism. In multi-layer models, this approach involves a Kraus–Turner type bulk mixed layer entrainment rate parameterization (e.g. Ni-

iler and Kraus, 1977; McCreary et al., 1996). While entrainment causes deepening of the mixed layer depth and material transfers across its base, an additional, albeit smaller, diffusive mixing is also introduced across the interfaces. The multi-level models, on the other hand, parameterize turbulent mixing through a variety of turbulence closure parameterizations (Varela et al., 1992; Radach and Moll, 1993; Sharpless and Tett, 1994; Oguz et al., 1996; Kuhn and Radach, 1997; Gregoire, et al., 1998; Levy et al., 1998; Zavaterelli et al., 2000).

This study is motivated by our ongoing efforts in Black Sea interdisciplinary studies devoted to developing a relatively simple, computationally efficient coupled circulation-ecosystem model, which does not sacrifice from the basics of the dynamics and biogeochemistry, and at the same time, is able to demonstrate a response compatible with computationally more demanding multi-level models. When a multi-layer approach with a relatively simpler vertical structure is desired to be used, the quality of model simulations depends crucially on appropriate representation of the vertical structure, hence the choice of the number of layers. To our knowledge, no study is available in the literature to quantify sensitivity of an ecosystem model to the choice of the vertical resolution of the biogeochemical structure. The present study addresses this issue and aims to identify the optimum number of vertical layers which can adequately provide observed ecosystem characteristics, and possess solutions comparable with the multi-level model. Our strategy will be first to show the capability of a particular multi-level model simulating the Black Sea interior basin ecosystem characteristics of the 1990s. This simulation is then repeated with multi-layer models providing a coarser representation of the upper layer water column. Although, this study is specifically designed for the Black Sea ecosystem, their results and implications should be fairly general and valid for other seas as well.

The paper is structured as follows. An overview of the observed ecosystem characteristics and recent modeling efforts relevant for this work is presented in Section 2. A general framework of the coupled, physical-ecosystem model formulation, for both multi-layer and multi-level cases, is then provided in Section 3. Some results from a particular multi-level model simulation and their comparison with the available observations are described in Section 4. It is followed in Section 5 by the corresponding simulations using the three and four layer models. A summary of results and conclusions are given in Section 6. Details of the entrainment formulation, and the biological source/sink terms of the ecosystem model are given in Appendices A and B, respectively.

2. Annual phytoplankton structure: an overview of observations and existing modeling efforts

A major, distinguishing feature of the Black Sea is considerable interannual/interdecadal variability of its ecosystem characteristics. The ecosystem has been under severe stress, with adverse changes since the late 1960s as a result of massive eutrophication, local pollution, population outbursts of opportunistic and gelatinous zooplankton species, and overfishing. Due to these perturbations, the ecosystem has shifted to a non-equilibrium state which has possessed different characteristics at different times. After the fish stocks declined precipitously by the late 1970s, the ecosystem structure and dynamics have been controlled mainly by opportunistic species (e.g. *Noctiluca*), and the gelatinous carnivores *Aurelia* in the l980s, *Mnemiopsis* during the late 1980s, and the two together during the 1990s (Oguz et al., 2001a). The annual phytoplankton structure has altered in this era depending on the nature of top-down grazing pressures introduced by these higher predators.

The available data and model simulations (Oguz et al., 2001a) indicated two distinct peaks in the phytoplankton biomass over the year when *Aurelia* was acting as a top predator. The first peak, occurring in March, was generated as a typical early spring bloom event following nutrient accumulation in the euphotic zone under strong winter mixing conditions. It was followed by subsequent peaks of the mesozooplankton and *Aurelia* biomass. As *Aurelia* grazed down the mesozooplankton, the phytoplankton had a

chance to recover and were subsequently consumed by the dinoflagellate *Nocticula*, thus giving rise to an increase in *Nocticula* biomass following those of the mesozooplankton and *Aurelia*. The second phytoplankton bloom event took place in October–November, coinciding with autumn rebounds in the *Aurelia* populations, and a subsequent decrease in the mesozooplankton stocks. Diminishing mesozooplankton grazing pressure caused once again a temporal increase in the phytoplankton biomass within the lower part of the euphotic zone experiencing sufficient light and nutrient to trigger primary production. A secondary *Noctiluca* bloom occurred later in November.

These blooms were shifted earlier by about 2 months when the system became controlled primarily by *Mnemiopsis* (Oguz et al., 2001a). The first bloom event of the year was initiated in January and reached its peak towards the end of February. Its earlier development was caused by the particular form of grazing pressure exerted by *Mnemiopsis*, which led to a complete depletion of micro and mesozooplankton and *Noctiluca* stocks during the late autumn, thus promoting early growth of the phytoplankton community in January. The winter phytoplankton bloom was followed by two subsequent blooms in April–May and July–August.

During the 1990s, the ecosystem was still dominated by *Mnemiopsis*, but its biomass decreased by two-to-three fold, compared with peak populations during the 1989–1991 period. Accordingly,

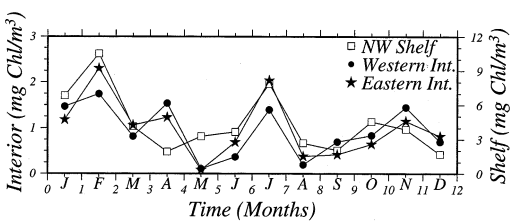

Fig. 1. The annual monthly averaged surface chlorophyll distribution (in mg^{-3}) at different regions of the Black Sea during the l990s when the ecosystem is controlled by the gelatinous carnivores (after Yilmaz et al., 1998). The open squares represent the data averaged over the northwestern shelf, the solid circles and solid stars for the interior parts of the western and eastern basins, respectively.

the winter, spring and summer blooms still exist in the system. There may be another bloom during the autumn season at times and regions where *Aurelia* exerts sufficiently strong grazing control on the lower trophic levels. The composite monthly mean surface chlorophyll data for the 1992–1996 period, averaged over various distinct regions of the sea, provide examples of such distinct peaks (Fig. 1). More details on Black Sea ecosystem characteristics during its different phases of succession and transformation can be found in Vedernikov and Demidov (1997), Kovalev et al. (1998), Yilmaz et al. (1998), Vinogradov et al. (1999), Nezlin et al. (1999), Mutlu (1999) and Kideys et al. (2000). As will be described in the following sections, our models are able to simulate the 1990s phytoplankton structure shown in Fig. 1.

3. Formulation of the models

The multi-level model introduces 40 vertical levels to approximate the vertical biogeochemical structure of the upper 100 m water column above the anoxic interface. The three-layer model simplifies this structure by introducing a seasonally varying 'mixed layer' at the surface, followed by the 'intermediate layer' forming the lower part of the euphotic zone below the seasonal thermocline, and the subsequent 'chemocline zone' representing the entire aphotic zone of the upper layer water column up to the anoxic interface. The latter layer acts as a nitrogen pool where sinking particulate materials are remineralized and converted to inorganic form, and then made available into the euphotic zone for the next cycle of new production. The first two layers characterize the region of major plankton production and organic matter synthesis. The three-layer structure is upgraded into the four-layer case by dividing the intermediate layer into two sub-layers. On the basis of some preliminary experiments, the position of the 5% light level, H_s, is chosen to divide the intermediate layer into two layers with comparable thicknesses. As shown in the following sections, the four-layer model yields an improved nitrogen cycling and biological production below the sea-

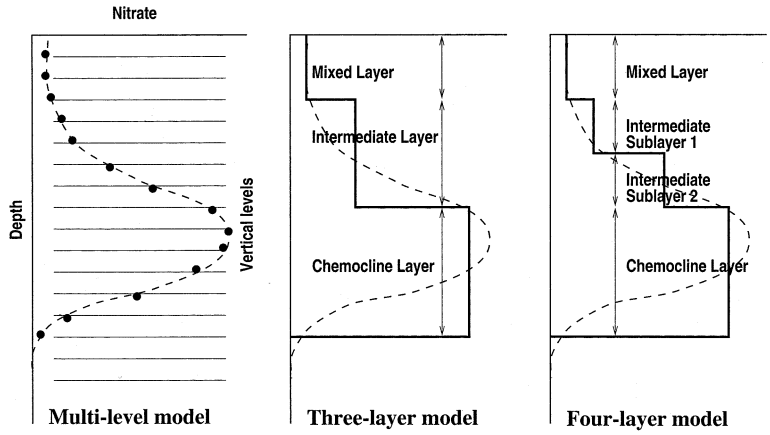

Fig. 2. The schematic representation of the vertical biogeochemical structure for the multi-level (left), the three-layer (middle) and the four-layer (right) models.

sonal thermocline. Using an idealized nitrate profile, typical vertical structures of the models are shown schematically in Fig. 2.

In the multi-layer models, the so-called 'dynamical mixed layer depth', $H_m^{(d)}$, is computed by:

$$\frac{\partial H_m^{(d)}}{\partial t} = W_e \tag{1}$$

where W_e denotes the entrainment velocity computed using a simplified Kraus–Turner type bulk mixed layer dynamics (see Appendix A). The 'biological mixed layer', H_m, is then introduced by:

$$H_m = \begin{cases} H_m^{(d)} \text{ if } H_m^{(d)} < H_e \\ H_e \text{ otherwise} \end{cases} \tag{2}$$

Eq. (2) implies that the maximum thickness of the mixed layer used in the biological models is limited by the euphotic layer. This criterion is set by assuming that deeper part of the mixed layer below the euphotic zone is biologically inactive in our models. The euphotic zone, defined by the thickness H_e, is treated as a slab. Its thickness is determined by the 1% light level for a given value of the water extinction coefficient. The thickness of the intermediate layer, H_i, is then found by the relation $H_i = H_e - H_m$. The difference between the total upper layer water column depth H_T (taken as 100 m) and the euphotic zone depth yields the thickness of the chemocline layer; $H_c = H_T - H_e$. In the four-layer case, the thicknesses of the intermediate sub-layers are computed by $H_{i1} = H_s - H_m$, $H_{i2} = H_e - H_s$. The basic properties of the multi-layer models are shown in Fig. 3a.

Both the multi-level and multi-layer models contain the same pelagic food web structure as well as the same formulation of biological processes and parameter setting. The pelagic food web, represented in the form of 10 aggregated compartments, comprises the small phytoplankton (P_s), large phytoplankton (P_l) (smaller and larger than 10 μm), microzooplankton (Z_s), mesozooplankton (Z_l), opportunistic heterotrophic dinoflagellate *Noctiluca scintillans* (Z_n), gelatinous carnivores *Aurelia aurita* (Z_a) and *Mnemiopsis leidyi* (Z_m). Labile pelagic detritus (D), nitrate (N), and ammonium (A) constitute other components of the aggregated ecosystem. Particulate organic material is converted directly to ammonium without explicitly considering the microbial loop mediating the decomposition and remineralization. This structure is similar to that given by Oguz et al. (2000, 2001a) except for the absence of dissolved organic nitrogen and bacterioplankton compartments. This simplification is, however, justified for the purpose of present paper, where we primarily deal with the simulation of annual phytoplankton structure. It is important to note that this foodweb constitutes a minimum configuration needed for a realistic simulation of the interior Black Sea annual plankton structure. Contribution of silicate to phytoplankton produc-

tion is omitted since silicate is not a major limiting nutrient for the interior Black Sea conditions. Nitrogen is, therefore, considered as the sole limiting macronutrient in the system. A schematic diagram of the model compartments and major biogeochemical processes included are shown in Fig. 3b.

The local temporal variations of all variables for both models are expressed by:

$$\frac{\partial F_j}{\partial t} = \chi_j(F) + \Re_j(F) \tag{3}$$

where t is time, ∂ is the partial derivative, F_j represents the concentration or biomass of any variable in layer or level j. $\Re(F)$ and $\chi_j(F)$ denote, respectively, a collection of the biological source–sink terms and the vertical transports associated with entrainment, diffusion and sinking. The forms of $\Re(F)$ for each state variable are described in Appendix B.

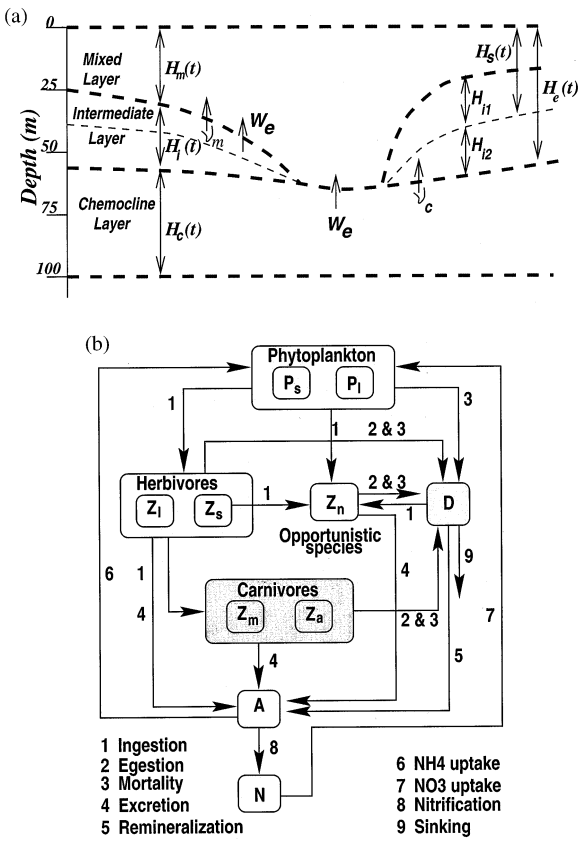

Fig. 3. The schematic diagram of the vertical structure and definition of some parameters of the multi-layer models. The schematic diagram of the compartments and biogeochemical processes included in the pelagic food web model.

Although the ecosystem structures for both the multi-level and multi-layer models are expressed in the form of Eq. (3), they differ in treatments of the vertical mixing, detritus sinking and light limitation terms. The multi-level model employs a time and depth-dependent vertical diffusion coefficients, whereas, the multi-layer models allow mixing and material exchanges across the layer interfaces through entrainment and diffusion. The layered models also treat particulate organic material sinking in the form of interfacial transfers, and represent the light limitation function as an averaged quantity over each layer. On the contrary, the multi-level model expresses these processes, respectively, in the advective form of exchanges between the vertical levels and a gradually varying smooth functional form.

The transport term $\chi(F)$ in Eq. (3) is expressed in the multi-level model by:

$$\chi(F) = \frac{\partial}{\partial z}\left[K_b \frac{\partial F}{\partial z} + w_s F\right] \tag{4}$$

where K_b is the vertical turbulent diffusivity, W_s represents the sinking velocity taken non-zero only for large phytoplankton and detrital material. The value of K_b within the mixed layer is determined from the level 2.5 Mellor–Yamada turbulence model (Oguz et al., 1996, 1999). Below the mixed layer, it attains a small, background value of 0.1 $cm^2\ s^{-1}$ up to 60 m, which then decreases linearly to 0.01 $cm^2\ s^{-1}$ at 75 m, and retains this value further below. This structure approximates reasonably well the observed profiles obtained by microstructure measurements (Gregg and Ozsoy, 1999) and is also consistent with the profiles estimated from the Gargett (1984) formula (cf., Oguz et al., 2001b).

Eq. (4) is complemented by the absence of turbulent and sinking fluxes at the surface ($z = 0$) and bottom ($z = -h_b$) boundaries of the model:

$$K_b \frac{\partial F}{\partial z} + w_s F = 0 \quad \text{at } z = 0 \text{ and } z = -h_b \tag{5}$$

Eq. (5) ensures remineralization of all particulate material within the model water column,

without any loss to the deeper waters. Moreover, no diffusive influx of nitrate and ammonium are allowed from the deep waters. This is because sub-pycnocline waters of the Black Sea are devoid of nitrate, but rich in ammonia which, however, can not contribute to the euphotic layer biological production. It is oxidized and lost completely near the anoxic interface as a result of complex redox reactions (Murray et al., 1995; Oguz et al., 2001b).

The net transport χ_m across the base of the mixed layer occurs as a combination of entrainment, vertical diffusion and sinking. In the presence of a finite intermediate layer (i.e. $H_i > 0$), it is expressed for the three-layer model by:

$$\chi_m = \frac{(\Theta(W_e)W_e + v_m)(F_i - F_m) - w_s F_m}{H_m} \quad (6)$$

where the Heaviside step function Θ is defined by $\Theta(W_e) = 1$ and $\Theta(-W_e) = 0$ if $W_e > 0$ (entrainment). v_m denotes the diffusion rate across the base of the mixed layer.

The net transport, χ_i, for the intermediate layer involves diffusion and sinking fluxes across its upper and lower boundaries:

$$\chi_i = \frac{v_c(F_c - F_i) - v_m(F_i - F_m) - w_s(F_i - F_m)}{H_i} \quad (7)$$

where v_c is the diffusion rate across the boundary between the intermediate and chemocline layers. The corresponding net transport for the chemocline zone is given by:

$$\chi_c = \frac{-v_c(F_c - F_i) + w_s F_i}{H_c} \quad (8)$$

Being consistent with Eq. (5), Eq. (8) specifies no exchange across its base, and assumes complete decoupling of the chemocline layer from deeper anoxic waters.

When the mixed layer deepens below the euphotic zone and the intermediate layer vanishes, we set $H_i = 0$, $F_i = F_m$, and $\chi_i = 0$. Under these conditions, the net flux at the base of the mixed layer is the same as in Eq. (6), except that F_I is replaced by F_c. Eq. (8) is then modified by changing F_I with F_m.

In the case of the four layer model, when the intermediate layer is represented by two sub-layers with thicknesses H_{i1} and H_{i2}, concentrations F_{i1} and F_{i2}, Eq. (6) is modified by replacing F_i with F_{i1}, and Eq. (8) by replacing F_I with F_{i2}. Eq. (7) is modified to the form:

$$\chi_{i1} = \frac{v_c(F_{i2} - F_{i1}) - v_m(F_{i1} - F_m) - w_s(F_{i1} - F_m)}{H_{i1}} \quad (9)$$

$$\chi_{i2} = \frac{v_c(F_c - F_{i2}) - v_m(F_{i2} - F_{i1}) - w_s(F_{i2} - F_{i1})}{H_{i2}} \quad (10)$$

The interfacial fluxes between the layers are further arranged according to deepening of the mixed layer over the second and the third layers.

3.1. Initial conditions, numerical procedure and parameter setting

The multi-level model is initialized by a vertically uniform nitrate profile of 3.5 mmol m^{-3}. The multi-layer models are initialized by specifying nitrate concentrations of 0.1, 1.0 and 6.0 mmol m^{-3} in the mixed layer, intermediate and chemocline layers, respectively. Both models assign initially small finite values for all other state variables. The multi-level model considers a constant detritus sinking velocity of 4 m per day. The multi-layer model also accepts the same value at the base of the mixed layer, but it is reduced to 1 m per day at the interface between the intermediate and the chemocline layers in order to allow a more efficient nitrogen recycling inside the intermediate layer.

The biogeochemical parameter values used for all models are listed in Tables 1–3. They are similar to those given earlier by Oguz et al. (2000, 2001a). The daily variations of wind stress magnitude $|\tau_0|$ the total heat flux Q_{tot}, and the photosynthetically available radiation (PAR) at the sea surface I_S are shown in Fig. 4. The data are based on basin averaged monthly climatologies used in our previous studies (Oguz et al., 1996, 1999, 2000, 2001a).

The equations are forwarded in time using the second order accurate leap-frog scheme. Its time splitting instability is controlled by smoothing the fields at every time step using the Aselin filter. The

Table 1
Parameters of the biological model used in the simulations

Parameter	Definition	Value
a	Photosynthesis efficiency parameter	0.01 m^2 W^{-1}
k_w	Light extinction coefficient	0.08 m^2 $mmol^{-1}$
k_c	Self-shading coefficient	0.07 m^{-1}
R_n	Half-saturation constant in nitrate uptake	0.5 mmol m^{-3}
R_a	Half-saturation constant in ammonium uptake	0.2 mmol m^{-3}
ψ	Ammonium inhibition parameter of nitrate uptake	3 m^3 $mmol^{-1}$
ε	Detritus decomposition rate	0.1 per day
Ω_a	Ammonium oxidation rate	0.1 per day
ν_m, ν_c	Diffusion rates	0.08 m per day
Δt	Time step	600 s
Z_{0a}	Background *Aurelia* biomass	0.1 mmol m^{-3}
Z_{0m}	Background *Mnemiopsis* biomass	0.1 mmol m^{-3}
t_g	Restoring time of the *Aurelia* and *Mnemiopsis* biomass	10 days

source/sink terms are solved implicitly wherever possible to avoid numerical instability during the time integration. The time step is taken to be 10 min for both models. The transient adjustment of the biological fields is accomplished to a large extent by the end of the second year. Due to the absence of any external sink or source (note that summation of all terms in Eqs. (B1), (B2), (B3), (B4), (B5), (B6), (B7) and (B8) is equal to zero), the final biological state reflects the distribution of the initial nitrate stocks among the living and non-living components of the ecosystem in response to the internal trophodynamic conditions set by the biological processes in the model.

Table 3
Food capture efficiency coefficients

Prey	Predator				
	Z_s	Z_l	Z_n	Z_a	Z_m
P_s	0.7	0.2	0.9	–	–
P_i	0.2	1.0	0.35	–	–
Z_s		0.7	0.2	0.2	0.2
Z_l	–	–	–	1.0	1.0
Z_n	–	0.2	–	–	–
D	1.0	0.7	0.2	–	

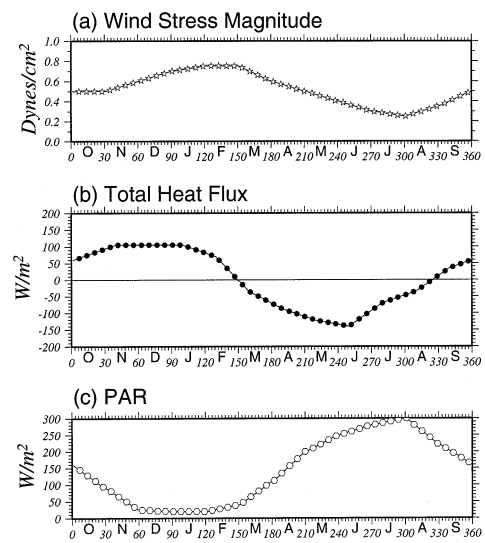

Fig. 4. The daily variations of climatiological (a) wind stress magnitude, (b) total heat flux, (c) photosynthetically available radiation used as forcing in the models.

Table 2
Parameters of the biological model used in the simulations

Parameter	Definition	P_l	P_s	Z_s	Z_l	Z_n	Z_a	Z_m
σ_i	Maximum growth rates	2.9	2.0	2.0	1.3	1.0	fitted	fitted
λ_i	Mortality rates	0.06	0.08	0.04	0.04	0.08	0.007	0.008
μ_i	Excretion rates	–	–	0.07	0.07	0.08	0.01	0.01
γ_i	Assimilation efficiencies	–	–	0.75	0.75	0.80	0.80	0.80
Q_{10}	Q_{10} parameter of $f(T)$	1.2	1.2	2.0	2.0	2.0	2.2	2.2
R_i	Half-saturation constant	–	–	0.5	0.4	0.5	0.7	0.50

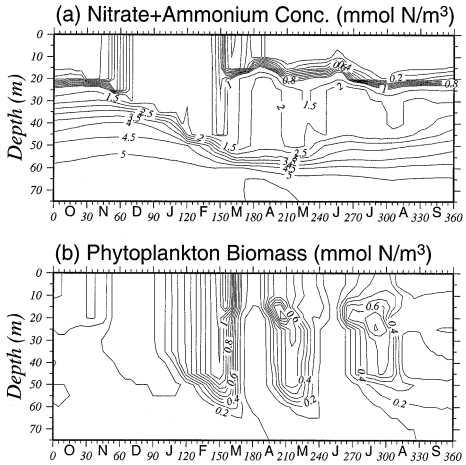

Fig. 5. The annual distributions of the (a) total nutrient (nitrate + ammonium), concentration, (b) total (large plus small) phytoplankton biomass within the upper 75 m of the water column throughout the year. They are expressed in the units of mmol Nm^{-3}. For nutrients, the contour interval is 0.5 for concentrations greater than 1.0, and 0.2 otherwise. For phytoplankton biomass, the contour interval is 0.1.

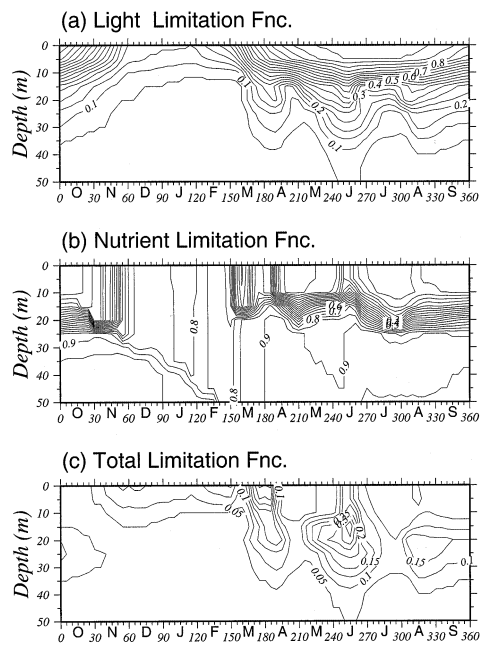

Fig. 6. The annual distributions of (a) the light limitation, (b) nutrient limitation, (c) total limitation functions within the upper 75 m of the water column throughout the year. The contour interval is 0.05 for all plots.

4. Multi-level model simulations

4.1. Vertical distributions

Fig. 5a, b show annual distributions of total inorganic nitrogen (nitrate plus ammonium) concentration and of total phytoplankton biomass ($P_S + P_l$) within the water column. Fig. 6a–c describe the corresponding distributions of the light, nutrient and net limitation functions. Inorganic nitrogen (Fig. 5a) reveals considerable seasonal variability within the upper 50 m implying that convective overturning, entrainment and nitrogen recycling mechanisms are most effective there. By the beginning of October, the mixed layer starts deepening due to autumn cooling and stronger wind forcing (see Fig. 6b in Oguz et al. 1999 for distribution of the vertical diffusion coefficient). The mixed layer nitrogen concentration then starts increasing gradually up to 1.0 mmol m^{-3} within the 25 m deep mixed layer by the end of December, and to 1.5 mmol m^{-3} over the upper 40 m by the end of January. Thereafter, nitrogen stored within the mixed layer is consumed rapidly in phytoplankton growth during February and early March. Primary production is limited by nitrate availability in October (Fig. 6a, b). Production starts as soon as the mixed layer accumulates sufficient nutrients from the deeper levels toward the end of October. The phytoplankton biomass increases to 0.3 mmol N m^{-3} during this event. It is terminated toward the end of November due to combined effects of mesozooplankton grazing pressure and gradual decrease in of the light availability (Fig. 6b). The January–February period is characterized by high nutrient, low light conditions (Fig. 6a and b, Fig. 4c). Due to the lack of predator grazing (i.e. no microzoo and mesozooplankton abundance in this period), a small increase in the light limitation (maximum value of the total limitation function goes up to 0.15; see Fig. 6c) triggers phytoplankton growth at the beginning of February. The phytoplankton biomass thus increase up to ~ 1.0 mmol/m^{-3} towards the end of February within the entire 50 m deep, well-mixed layer. The important point to note here is that even though PAR is available for only the upper 15 m of the water column in this

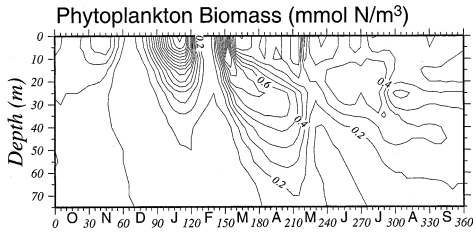

Fig. 7. The annual distribution of total (large plus small) phytoplankton biomass (mmol N m^{-3}) within the upper 75 m of the water column throughout the year for the case of constant vertical diffusion coefficient of $K_b = 1.0$ cm^2 s^{-1} used in the simulations. The contour interval is 0.1.

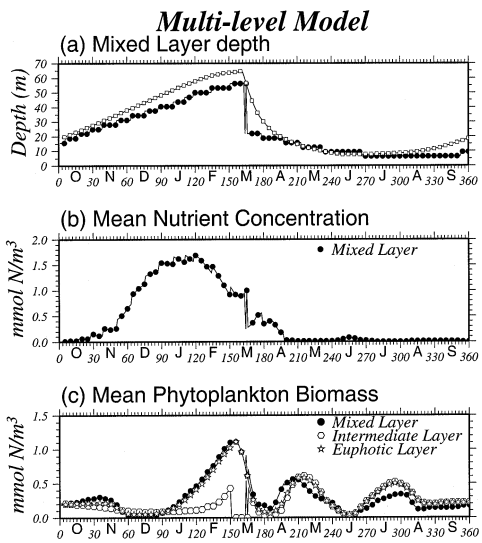

Fig. 8. The annual distributions of the (a) mixed layer depth (solid circles), (b) total nutrient (nitrate + ammonium) concentration, (c) total (large plus small) phytoplankton biomass within the mixed and intermediate layers of the multi-level model. The dynamical mixed layer depth variations computed by the multi-layered models (open squares) are also included for comparison.

period (due primarily to low intensity surface PAR), strong winter vertical mixing generated by cooling and strong wind forcing (Fig. 4a and b) redistributes phytoplankton cells over the entire mixed layer. In the absence of such a strong vertical mixing, however, the biomass is confined to a narrower region near the surface identified by the non-zero values of the light limitation function. Fig. 7 describes the phytoplankton distribution computed when the last year of the previous simulation is repeated using a weaker, constant eddy diffusion coefficient of $K_b = 1.0$ cm^2 s^{-1} only for the phytoplankton equations. The single and continuous bloom event of the previous simulation shown in Fig. 5b is now divided into two separate and isolated events. The first takes place in January and is clearly confined within the upper 20 m zone below which receives negligible solar radiation during this period. The next bloom event starts 2 weeks after the termination of the first one, and attains its peak at the end of February. The bloom is most intensified within the upper 15 m zone due to the additional contribution of recycled nutrients from the previous event.

A temporary, short-term increase in the near-surface phytoplankton biomass takes place during the first half of March (Fig. 5b) as a consequence of efficient nitrogen recycling associated with the ongoing phytoplankton bloom event. Thereafter, the nitrogen content of the near-surface levels are gradually depleted in April. The mixed layer then remains completely devoid of nitrogen until the next October. Further below, nitrogen concentrations of about 1.5–2.0 mmol m^{-3} extend uniformly to the permanent nitracline zone. The relative increase in the summer subsurface nitrogen concentration by about 0.5–1.0 mmol m^{-3} with respect to its values prior to the early spring bloom signifies contribution of the recycling process. This extra nitrogen supports two subsurface phytoplankton production events during late April–May and late July–August (Fig. 5b). Timing of these blooms is controlled by the particular sequence of prey–predator interactions introduced by the life cycles and population dynamics of gelatinous carnivores in the ecosystem. The subject of top–down grazing control operating in the Black Sea ecosystem is beyond the scope of the present paper. It was described thoroughly in Oguz et al. (2001a).

4.2. Layer-averaged properties

The average nutrient concentrations and phytoplankton biomass distributions computed over the mixed and the intermediate layers of the multi-

level model are shown in Fig. 8. Also given in the same figure are the mixed layer variations computed by both the Mellor–Yamada turbulence closure scheme and the Kraus–Turner bulk mixed layer parameterizations of the multi-layer models. The mixed layer depth in the multi-level model is computed at each time step diagnostically as the depth at which the vertical diffusivity drops to its background value of 0.1 $cm^2\ s^{-1}$ This criterion was found to be a good tracer for the base of the mixed layer, and be consistent with the depths of thermocline and nitracline predicted by the model (cf., Fig. 6b in Oguz et al., 1999). The mixed layer thickness of the multi-level model (Fig. 8a) possesses an almost linear trend of increase during the autumn and winter seasons characterized by buoyancy—(i.e. cooling) and wind-induced mixing. Its deepest position attains about 60 m towards the first week of March. As the winds weaken and cooling stops (c.f. Fig. 4), mixing ceases and the mixed layer undergoes an abrupt shallowing to about 20 m within a day. It continues to shoal afterwards in the spring and summer periods of weak wind forcing and strong heating. The shallowest position is around 7 m during July–August. This structure compares well with the so-called 'the dynamical mixed layer' (see open squares in Fig. 8a) predicted by the bulk mixed layer formulation (Eq. (2)).

Clearly, the deepening phase of the mixed layer is accompanied by nutrient entrainment from the subsurface levels. More nutrients are transported from the sub-surface nitrate pool as the mixed layer deepens further into the nitrogen rich lower levels. Consequently, the mixed layer averaged nitrogen concentration increases up to 1.6 mmol m^{-3} during January (Fig. 8b) prior to initiation of the phytoplankton bloom. Afterwards, as the available nitrogen stock in the mixed layer is consumed during the phytoplankton bloom, mixed layer average nitrogen concentration decreases at the expense of an increase in the phytoplankton biomass (Fig. 8c). As described earlier, the mixed layer does not store additional nitrogen from April to November. Nitrogen made available by recycling is consumed during the spring and summer bloom events. However, because the mixed layer is quite shallow during this period (less than 10 m), the contribution of these blooms to the overall euphotic zone budget is negligible. The production below the mixed layer provides the major contribution to the euphotic zone during the spring and summer months.

The magnitude and timing of the mixed layer phytoplankton biomass peaks agree reasonably well with the interior basin monthly mean surface chlorophyll data given previously in Fig. 1, even though the predicted autumn bloom event is not as strong as observed in the data. As we shall see in the next section, the four layer model reproduces this event better. Assuming a carbon to nitrogen ratio C:N = 8.0, chlorophyll to carbon ratio Chl:C = 50, 1 mmol N corresponds roughly to 2 mg Chl, which is a typical surface chlorophyll peak value for the interior basin, where this model is most relevant. The model-data consistency becomes even better if the data are processed in the form of weekly averages (unpublished data; Oleg Yunev, personal communication).

5. Multi-layer model simulations

In this section, following a brief description of the mixed layer structure predicted by the Kraus–Turner type bulk entrainment formulation (cf., Eq. (A1)), the nutrient concentration and phytoplankton biomass predictions of the three and four layer models are presented, and compared with the corresponding layer-averaged properties of the multi-level model.

As already noted above, the dynamical mixed layer depth structure computed by the bulk formulation in the layered models is quite comparable with that obtained from the multi-level model (see Fig. 8a). Once again, the mixed layer thickens linearly from 20 m depth at the beginning of October to approximately 65 m depth at the end of February. As soon as the mixing ceases and detrainment begins, the mixed layer depth reduces by about 30 m during March, and more gradually later on. In the transition period from mid-March to mid-April, the mixed layer variations predicted by the level and layer models, therefore, differ slightly. Their consistency is, however, much better during the rest of the year except for some

overestimation by about 10 m during the winter months. Our sensitivity experiments indicated that a much better match can, in fact, be achieved between these two winter mixed layer structures by altering some parameters of the entrainment formulation slightly. This, however, implicitly implies reducing the entrainment rate, which then gives rise to somewhat lower nutrient entrainment and a weaker winter bloom simulation. The structure shown here, therefore, reflects a compromise. On the other hand, the exact reproduction of the winter mixed layer structure by the layer model is irrelevant, since the part of mixed layer below the euphotic zone is not biologically important in the layered models. As recalled from Section 3, when the mixed layer depth predicted by the dynamical model exceeds the thickness of the euphotic zone (i.e. $H_m^d - H_e$) the mixed layer depth is truncated by the depth of the euphotic zone (cf., Eq. (2)).

5.1. Three-layer model structure

The layer thicknesses, nutrient concentrations and phytoplankton biomass distributions computed by the three layer model are shown in Fig. 9. During the autumn phase of vertical mixing, when the mixed layer is still shallower than the euphotic zone (Fig. 9a), vertical diffusion provides the only source of nutrient supply from the chemocline to the intermediate layer. This process leads to a gradual increase of the intermediate layer nutrient concentration up to 1.5 mmol m^{-3} by the end of December (Fig. 9b). On the other hand, the relatively limited nutrient stocks of the intermediate layer during this phase allow only a limited supply into the mixed layer since the rate of nutrient transfer is proportional to the concentration differences between the layers. As soon as the dynamical mixed layer (see the curve with open squares in Fig. 8a) becomes thicker than the euphotic zone by early January (Fig. 9a), its nitrogen content increases more abruptly since it establishes a direct contact with the chemocline layer comprising much higher nutrient concentrations. The intermediate layer is absorbed into the mixed layer during this phase and its nutrients become a part of the mixed layer stocks. However, because its thickness tends to vanish as the mixed layer thickens, its layer integrated nutrient content provides only negligible contribution to the mixed layer budget. The time at which H_i vanishes in Fig. 9a corresponds with the sudden drop of intermediate layer nutrient concentrations to zero in Fig. 9b. Similarly, the day at which this layer recovers again during the mixed layer shallowing phase is marked by a sudden increase of its nutrient concentration.

The nutrient concentration in the mixed layer attains a maximum value of about 1.4 mmol m^{-3} at the end of January. In fact, January signals initiation of the winter bloom and nutrient consumption simultaneously to support this event. The phytoplankton biomass increase gradually up to 1.3 mmol m^{-3} by the end of February. The bloom event terminates within the first half of March once the nutrients are depleted and more active grazing pressure is exerted on phytoplankton by the herbivorous zooplankton and the opportunistic species *Noctiluca*. A secondary, regeneration-based production peak takes place towards the end of March as a response to nutrient recycling inside this layer.

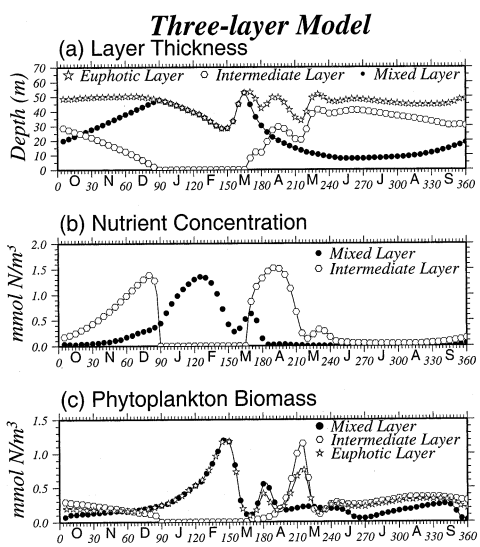

Fig. 9. The annual distributions of the (a) mixed, intermediate and euphotic layer depths, (b) total nutrient (nitrate + ammonium) concentrations, (c) total (large plus small) phytoplankton biomass within the mixed and intermediate layers of the three layer model.

Once the mixed layer becomes shallower than the euphotic zone after mid-March (Fig. 9a), organic matter production and nutrient recycling rapidly build up nutrients within the intermediate layer up to 1.7 mmol m^{-3} by the first half of April. They then trigger a short term subsurface bloom event with maximum biomass around 1.0 mmol m^{-3} at the end of April. Following a decline in both nutrient stocks and phytoplankton biomass in May, both the intermediate and mixed layers maintain some production at a rather steady level during the entire summer. However, since the mixed layer is shallower than 10 m at this time of the year (see Fig. 9a), the euphotic zone budget is predominantly controlled by the production in the intermediate layer (Fig. 9c). This production is supported both by recycling of nutrients inside the layer as well as additional diffusive input from the chemocline layer. As noted in Fig. 9b, additional nutrients are not accumulated during these events; instead they are consumed immediately. When compared with the results of the multi-level model simulation shown earlier, the three-layer model achieves reasonable success in capturing the main features of biological production and nutrient cycling. The winter bloom is predicted quite well. The April–May bloom of the intermediate layer, which takes place almost simultaneously with the mixed layer bloom in the multi-level model (Fig. 8c), is also produced with correct timing and magnitude (Fig. 9c). The three-layer model produces the mixed and intermediate layer blooms with 1 month time lag, and their durations are somewhat shorter than those predicted by the multi-level model. The main deficiency of the three-layer model is, however, the presence of a rather continuous low level summer production instead of an isolated and stronger event shown by observations in July–August (cf., Fig. 1). As already mentioned above, the reason for the absence of the summer bloom in the three layer model is the lack of sufficient nutrient accumulation within the intermediate layer. The nutrients used to produce earlier the April–May bloom are not recycled inside this layer as efficiently as in the multi-level model. The partial lost to the chemocline layer in the form of particulate organic matter are not also re-supplied back efficiently by diffusion. The efficiency of nutrient recycling in the multi-level model becomes evident by comparing its intermediate level concentrations of about 1.5–2.0 mmol m^{-3} in Fig. 5a with respect to the corresponding values of about 0.1 mmol m^{-3} in Fig. 9b. In the multi-level model, the May bloom follows the nutrient accumulation (greater than 2.0 mmol m^{-3}) within the 20–50 m zone right after the March bloom. The nutrient content decreases within the bloom period, but it then increases again over 2.0 mmol m^{-3} in June prior to the July–August bloom. Moreover, representing the relatively broad intermediate layer with ~ 3 m vertical grid spacing allows different parts of the intermediate layer to contribute to phytoplankton growth at different periods. The three layer configuration, however, cannot support such fine details of the multi-level model. But, as we will show next, representing the intermediate layer in two sub-layers captures some features of the multi-level model and provides some improvement on the three-layer model results.

5.2. Four-layer model structure

The four-layer model results are shown in Fig. 10 and Fig. 11. We recall that the interface between the two sub-layers of the intermediate layer is chosen as the depth of the 5% light level, since it lies roughly midway between the mixed layer and the base of the euphotic zone (Fig. 10a). Comparing the nutrient and phytoplankton distributions (Fig. 10b and c) with those of the three-layer model shown in Fig. 9b and c suggests that the intermediate layer now is able to maintain more efficient recycling and acquires extra summer nutrients of the order of 1.0 mmol m^{-3} as in the multi-level model. Once again, the model is able to predict the winter bloom quite consistently with the multi-level model. The biomass is predicted slightly higher than the other models, because of the entrainment of the extra nutrients available in the intermediate layer prior to the entrainment from the chemocline. It is followed by additional blooms both in the upper and lower parts of the intermediate layers simultaneously during April–May (Fig. 11b). They, therefore,

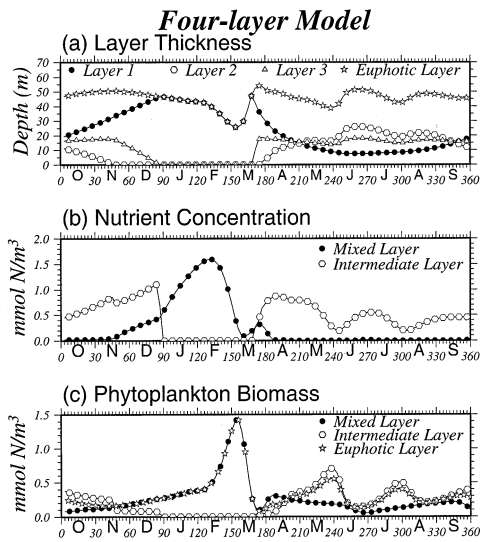

Fig. 10. The annual distributions of the (a) mixed, intermediate and euphotic layer depths, (b) total nutrient (nitrate + ammonium) concentrations, (c) total (large plus small) phytoplankton biomass within the mixed and intermediate layers of the four layer model.

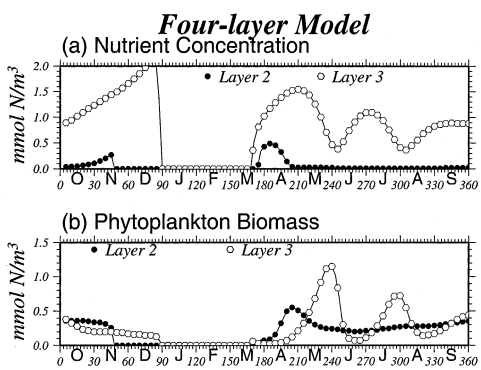

Fig. 11. The annual distributions of the (a) total nutrient (nitrate + ammonium) concentrations, (b) total (large plus small) phytoplankton biomass within the second and third layers of the four layer model.

give rise to a more extended bloom period (Fig. 10c), which is somewhat similar to the multi-level model case even though its peak period differs slightly from that shown in Fig. 8c. During the rest of the summer, the nutrients in the second layer are already depleted, and this layer does not contribute to biological production any more (Fig. 11a), as in the single intermediate layer case of the three layer system. On the other hand, some nutrients are still present within the third layer, and provide a subsequent bloom in July similar to the multi-level model case (Fig. 11a and b). Further recycling of nutrients within this layer together with the top–down control by *Aurelia* promote a subsequent bloom event later in the September–October period. Afterwards, the intermediate layer biological activities are taken over by the mixed layer due to its gradually enhancing mixing activities during the subsequent autumn and winter months.

In the three layer model, the choice of diffusion rate is found to be critical for the amount of nutrients supplied into the intermediate layer, and subsequently for the phytoplankton biomass structure during the summer months. An experiment with 50% higher diffusion rates of $v_c = v_m$ m per day shows more pronounced phytoplankton biomass peak during the August–September period (Fig. 12a). But, in this case, the structure of the March–April blooms changes to some extent as compared with the one shown in Fig. 9c. On the other hand, because the four layer model promotes more efficient nutrient cycling within the intermediate layer, the same diffusion rate does not lead to any appreciable change in the intermediate layer phytoplankton structure in the summer months (Fig. 12b).

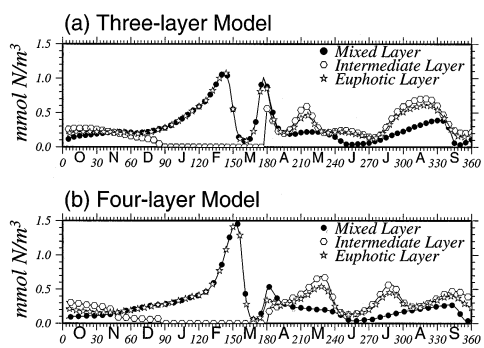

Fig. 12. The annual distributions of the total (large plus small) phytoplankton biomass within the mixed and intermediate layers computed using the vertical diffusion rate of 0.12 m per day for (a) the three layer, (b) the four layer models.

6. Summary and conclusions

The present work investigates feasibility of simulating euphotic zone biological characteristics using a relatively simple multi-layer model, as an alternative to a more complex and computationally more demanding multi-level model approach. Two particular types of alternative layer configurations are investigated. The first one represents the upper layer water column of the Black Sea above the anoxic interface in the form of three interactive layers. The euphotic zone is represented by the mixed layer at the surface and the intermediate layer beneath the seasonal thermocline. The third one covers the aphotic zone further below. It serves as a nutrient reservoir to provide new nutrients to the euphotic zone by entrainment and diffusion. The second choice is the four layer configuration in which the thermocline region is resolved by two layers, instead of one single and thicker layer of the three-layer case.

Using a set of common biogeochemical parameters for all models, we first demonstrated how the multi-level model can predict adequately the observed phytoplankton distribution in the form of a series of peaks during the year. No sensitivity study on the dependence of model simulations to various biological parameters is carried out, since it was explored previously elsewhere (Oguz et al., 2000, 2001a). We, however, tested the response of the multi-layer models to some particular physical parameters which are assigned as free parameters. Namely, the values of entrainment velocity, vertical diffusion rate, detritus sinking velocity through the layer interfaces, temperatures of the subsurface layers, etc. are varied within their given realistic/expected ranges. It is found that the layered models are not overly sensitive to these parameters, except the diffusion rate. It is possible to state that the four layer model possesses somewhat more robust character than its three layer alternative.

The four-layer representation of the upper layer water column indeed provides a yearly biological structure similar to that simulated by the multi-level model. The subsurface blooms owe their existence to the presence of nutrient recycling with almost comparable efficiency with the multi-level model. On the other hand, the three-layer model has unavoidably a poorer recycling capability. This deficiency may, however, be compensated to some extent by prescribing a higher rate of diffusion to allow more nutrient transfer from the chemocline layer.

Although, both the layer and level models predict the winter bloom quite well, its formation and vertical extension have some interesting differences and deserve some further comments. In the multi-level model, the winter bloom is originated within the upper 15–20 m irradiated part of the mixed layer having non-zero values of the light limitation function. It is then uniformly distributed over the entire mixed layer of about 50 m due to vigorous convective overturning generated by strong wind and cooling-induced mixing. In the multi-layer models, on the other hand, the light limitation function, averaged over the mixed layer, promotes bloom generation within the entire mixed layer. This raises the issue of resolving the mixed layer in the form of several sub-layers so that the mixed layer average light limitation function may be represented somewhat more realistically. Our experiments with the mixed layer resolved in the form of three equidistant sub-layers, however, indicated no additional apparent advantage. Thus the four layer structure emerges as the best and simplest multi-layer configuration which may provide almost all major features of the ecosystem simulated by its multi-level counterpart.

Acknowledgements

This work is a contribution to the Black Sea-ODBMS Project sponsored by the NATO Science for Peace Program. It is supported in part by the NSF Grant OCE-9906656 to Temel Oguz and Paola Malanotte-Rizzoli, and OCE-9908092 to Hugh W. Ducklow. Temel Oguz also acknowledges the NATO Linkage Grant EST.CLG 975821, which enabled him to interact with various scientists from other Black Sea countries. We thank the Editor, S.E. Jorgensen, and a reviewer for their thoughtful and constructive comments.

Appendix A. Entrainment formulation

The entrainment rate, W_e, is computed as in Niiler and Kraus (1977) by:

$$\Theta(W_e)W_e b_m H_m = 2mu_*^2 + H_m B_0[1-\lambda\Theta(W_e)] \quad \text{(A1)}$$

where $u_*^2 = |\tau_0|/\rho_0$ denotes the friction velocity square with $|\tau_0|$ representing magnitude of the wind stress, $b_m = g(\Delta\rho/\rho_0)$ is the buoyancy at the base of the mixed layer, and B_0 is the total buoyancy flux through the surface expressed by:

$$B_0 = g\left[\frac{\alpha Q_{tot}}{\rho_0 c_p} + \beta S_0(e-p)\right] \quad \text{(A2)}$$

B_0 varies temporally due to the total surface heat flux $Q_{tot}(>0$ for cooling), and the fresh water flux given by the surface salinity S_0 and the evaporation minus precipitation rate $(e-p)$. The definition and values of all other parameters are given in following table.

The definition of some functions used in the biological model are as follows:

Definition	Function
Light intensity at depth z	$I(z,\ t) = \mathrm{I_s exp}[-k_w z - k_c\ (\mathrm{P_f}+\mathrm{P_d})$
Light limitation function	$\alpha(I) = \tanh[aI\ (z,\ t)]\mathrm{dz}$
Layer averaged light limitation function	$\alpha(I)_\mathrm{I} = 1/H_i \int \tanh[aI(z,\ t)]\mathrm{dz}$
Ammonium limitation function	$\beta_a(\mathrm{A}) = \mathrm{A}/(R_a+\mathrm{A})$
Nitrate limitation function	$\beta_n(\mathrm{N}) = [\mathrm{N}/(R_n+\mathrm{N})]\exp(-\psi\mathrm{A})$
Total nitrogen limitation function	$\beta_t(\mathrm{N},\ \mathrm{A}) = \beta_n(\mathrm{N}) + \beta_a(\mathrm{A})$
Temperature limitation function	$f(T) = \mathrm{Q}_{10}^{(T-20)/10}$
Overall limitation function	$\Phi = \alpha(I)\beta_t(\mathrm{N},\ \mathrm{A})f(T)$
Grazing functions	$G_i(\psi_j) = \sigma_i(a_j\psi_j/R_i + \Sigma a_n\psi_n)$
	$G_i(\psi_j) = \sigma_i(t)\psi_j$

Strictly speaking, $\Delta\rho$ defines the density difference between the mixed layer and at its base. Since we do not specifically predict the mixed layer density in the present model, and since the base of the mixed layer characterizes the seasonal thermocline with large density changes, a precise way of specifying $\Delta\rho$ is not possible. Here, on the basis of several experiments using an independent mixed layer model with a layer linearly stratified density structure below, we set $\Delta\rho = 2$ kg m^{-3} throughout the year. Eq. (A1) describes a balance between the rate of potential energy increase of the upper ocean due to buoyancy inputs (the left hand side) and the net rate of turbulent kinetic energy production due to wind stirring, cooling and net evaporative loss (the right hand side). One process which is omitted in the present parameterization is the contribution of interfacial shear instability to the turbulence energy production. This term has an important contribution only when there is a high velocity shear [O(1 m s^{-1})] across the interface, which does not exist generally in the Black Sea. The contribution of the penetrative solar radiation on the turbulent energy production/destruction is much smaller than the other factors, and thus neglected in the present formulation. When there is no sufficient surface-generated turbulent kinetic energy at the base of the mixed layer to overcome stabilizing effect of the surface buoyancy flux (i.e. the right hand side of Eq. (A1) is zero or negative), the mixed layer retreats to shallower depths. The detrainment rate defining the time rate of change of mixed layer retreat is computed at each time step by:

$$W_e = \frac{H_{mo} - H_m(t-\Delta t)}{2\Delta t} \quad \text{(A3)}$$

where Δt is the time step, $H_m(t-\Delta t)$ is the thickness of the mixed layer at the previous time step. H_{mo} denotes the mixed layer depth (the so-called Monin–Obukhov depth) derived from a balance between wind-induced turbulence kinetic energy production and its loss due to surface heating (see McCreary et al., 1993). Thus, setting the right hand side of Eq. (A1) to zero yields:

$$H_m \equiv H_{mo} = -\left[\frac{2mu_*^2}{B_0}\right] \quad \text{(A4)}$$

Appendix B. Biological source/sink terms

For each vertical level or layer, the biological source/sink terms for both large and small phytoplankton groups are:

$$\Re(P_k) = \sigma_k \Phi P_k - [G_s(P_k)Z_s + G_l(P_k)Z_l + G_n(P_k)Z_n] - \lambda_k P_k^2 \quad \text{(B1)}$$

where the subscript k denotes either l or s. Accordingly, temporal changes in phytoplankton standing stocks are controlled by the primary production (the first term), zooplankton grazing losses (the second, third and fourth terms) and physiological mortality (the last term). The mortality term also includes the effect of exudation, and is expressed in a quadratic form for stability reasons. Primary production is modeled as products of the maximum specific growth rate σ_k, the overall limitation function Φ, and the phytoplankton biomass P_k. Φ is defined by the products of the individual limitation functions for light $\alpha(I)$, nutrient $\beta_t(N, A)$, and temperature $f(T)$. Nutrient limitation is expressed according to Monod uptake kinetics as the sum of nitrate and ammonium limitation functions in which preferential uptake of ammonium over nitrate is enforced. Inclusion of both ammonium and nitrate allows explicit determination of both 'new' and 'regenerated' production. For further details on the phytoplankton growth formulation, we refer to the following table.

The definition and values of the parameters used in the entrainment formulation are as follows:

Parameter	Definition	Value
ρ_0	Reference density	1017 kg m^{-3}
G	Gravitational constant	9.81 m s^{-2}
M	Efficiency of wind mixing	1.0
$\Delta\rho_0$	Density difference at the base of the mixed layer	2 kg m^{-3}
C_p	Specific heat of water	4025 J kg^{-1} per °C
α_t	Heat expansion coefficient	0.00025 per °C
β_s	Salt expansion coefficient	0.0007
λ	Fraction of TKE dissipation	0.3

The microzooplankton and mesozooplankton biomass are controlled by ingestion and egestion (which are assimilated and unassimilated parts of grazing, respectively), predation as well as mortality and excretion. They are expressed by:

$$\Re(Z_s) = \gamma_s[G_s(P_s) + G_s(P_l) + G_s(D)]Z_s - G_l(Z_s)Z_l - G_n(Z_s)Z_n - G_m(Z_s)Z_m - G_a(Z_s)Z_a - \mu_s Z_s - \lambda_s Z_s \quad \text{(B2)}$$

$$\Re(Z_l) = \gamma_l[G_l(P_s) + G_l(P_l) + G_l(D) + G_l(Z_s) + G_l(Z_n)]Z_l - G_m(Z_l)Z_m - G_a(Z_l)Z_a - \mu_l Z_l - \lambda_l Z_l \quad \text{(B3)}$$

In Eqs. (B2) and (B3), the first three terms within the first square brackets describe consumption of small and large phytoplankton, and detritus by micro- and mesozooplankton, respectively. The subsequent two terms within Eq. (B3)

represent ingestion of microzooplankton and *Noctiluca* by mesozooplankton. They are followed by the group of terms representing predation of micro- and mesozooplankton by gelatinous carnivores (*Aurelia* and *Mnemiopsis*), and additionally by mesozooplankton and *Noctiluca* in the case of microzooplankton Eq. (B2). The last two terms describe excretion and mortality, respectively, which are both expressed in the linear form. Grazing/predation are represented by the Michaelis–Menten functional form for micro-, and mesozooplankton and *Noctiluca*, and in the linear form for the gelatinous carnivore groups (see Table B1).

Noctiluca assimilate phytoplankton, microzooplankton and detritus with an efficiency of γ_n as described by the terms within the first square brackets of Eq. (B4). The subsequent terms indicate grazing of *Noctiluca* by mesozooplankton, their excretion and mortality, respectively.

$$\Re(Z_n) = \gamma_n[G_n(Z_s) + G_n(P_s) + G_n(P_l) + G_n(P_l) + G_n(D)]Z_n - G_n(Z_n)Z_l - \mu_n Z_n - \lambda_n Z_n \quad \text{(B4)}$$

The equations describing the source/sink terms for *Aurelia* and *Mnemiopsis* are given by:

$$\Re(Z_k) = \gamma_k[G_k(Z_s) + G_k(Z_l)](Z_k - \mu_k Z_k - \lambda_k Z_k + (Z_{k0} - Z_k)/t_g) \quad \text{(B5)}$$

where the subscript k denotes either a for *Aurelia* or m for *Mnemiopsis*. The first two terms represent ingestion of microzoo- and mesozooplankton by these gelatinous carnivores, whereas the subsequent two give their excretion and mortality. The last term indicate that gelatinous carnivore biomass does not drop below a small background value Z_{k0}.

Fecal pallets constituting unassimilated parts of the food grazed by zooplankton groups (the terms inside the first five square brackets in Eq. (B5)), as well as the phytoplankton and zooplankton mortalities (terms inside the sixth square brackets) form detritus sources. Detrital material are consumed by microzoo-, mesozooplankton and *Noctiluca*, and transformed to ammonium at a rate *e*. They are given by the last four terms in Eq. (B6).

$$\begin{aligned}\Re(D) = {} & (1-\gamma_l)[G_l(P_s) + G_l(P_l) + G_l(Z_s) + G_l(Z_n)G_l(D)]Z_l + (1-\gamma_s)[G_s(P_s) + G_s(P_l) + G_l(D)]Z_s \\ & + (1-\gamma_m)[G_m(Z_s) + G_m(Z_l)]Z_m \\ & + (1-\gamma_n)[G_n(Z_s) + G_n(P_s) + G_n(P_l) + G_l(D)]Z_n + (1-\gamma_a)[G_a(Z_s) + G_a(Z_l)]Z_a \\ & + [\lambda_s P_s^2 + \lambda_l P_l^2 + \lambda_s Z_s + \lambda_l Z_l + \lambda_m Z_m + \lambda_a Z_a + \lambda_n Z_n] - \gamma_n G_n(D)Z_n \\ & - \gamma_s G_s(D)Z_s - \gamma_l G_l(D)Z_l - \varepsilon D \end{aligned} \quad \text{(B6)}$$

Remineralization of detrital material and zooplankton excretion are two processes contributing to the increase in ammonium concentrations. The losses are the ammonium uptake during primary production and oxidation to nitrate. They are given by:

$$\Re(A) = -\Phi\left(\frac{\beta_a}{\beta_t}\right)(\sigma_s P_s + \sigma_l P_l) - \Omega_a A + \varepsilon D + [\mu_s Z_s + \mu_s Z_s + \mu_n Z_n + \mu_m Z_m + \mu_a Z_a] \quad \text{(B7)}$$

Similarly, the difference between phytoplankton uptake and nitrification controls the change in the nitrate stocks. The source/sink terms for the nitrate equation are then written by:

$$\Re(N) = -\Phi\left(\frac{\beta_n}{\beta_t}\right)(\sigma_s P_s + \sigma_l P_l) + \Omega_a A \quad \text{(B8)}$$

References

Aknes, D.L., Lie, U., 1990. A coupled physical-biological pelagic model of a shallow sill fjord. Estuarine, Coastal Shelf Sci. 31, 459–486.

Anderson, T.R., Williams, B., P.J., 1998. Modeling the seasonal cycle of dissolved organic carbon at station E in the English Channel. Estuarine, Coastal and Shelf Science 46, 93–109.

Dadou, I., Garcon, V., Andersen, V., Flieri, G.R., Davies, C.S., 1996. Impact of the north equatorial current meandering on a pelagic ecosystem: a modeling approach. J. Mar. Res. 54, 311–342.

Doney, S.C., Glover, D.M., Najjar, R.G., 1996. A new coupled, one-dimensional biological-physical model for the upper ocean: Applications to the JGOFS Bermuda Atlantic Time-Series Study (BATS) site. Deep Sea Res. II 43, 591–624.

Eigenheer, A., Wilfried, K., Radach, G., 1996. On the sensitivity of ecosystem box model simulations on mixed layer depth estimates. Deep-Sea Res. I 43, 1011–1027.

Evans, G.T., Parslow, J.S., 1985. A model of annual plankton cycles. Biol. Oceanogr. 3, 328–347.

Fasham, M.J.R., Ducklow, H.W., Mckelvie, S.M., 1990. A nitrogen-based model of plankton dynamics in the oceanic mixed layer. J. Mar. Res. 48, 591–639.

Franks, P.J.S., Wroblewski, J.S., Flierl, G.R., 1986. Behaviour of a simple plankton model with food-level accumulation by herbivores. Mar. Biol. 91, 121–129.

Gargett, A.E., 1984. Vertical eddy diffusivity in the ocean interior. J. Mar. Res. 42, 359–393.

Gregg, M.C., Ozsoy, E., 1999. Mixing on the Black Sea shelf north of the Bosphorus. Geophys. Res. Lett. 26, 1869–1872.

Gregoire, M., Beckers, J.M., Nihoul, J.C.J., Stanev, E., 1998. Reconnaissance of the main Black Sea's ecohydrodynamics by means of a 3D interdisciplinary model. J. Mar. Syst. 16, 85–106.

Hurtt, G.C., Armstrong, R.A., 1996. A pelagic ecosystem model calibrated with BATS data. Deep Sea Res. II 43, 653–683.

Jamart, B.M., Winter, D.F., Banse, K., Anderson, G.C., Lam, R.K., 1977. A theoretical study of phytoplankton growth and nutrient distribution in the Pacific Ocean off the northwestern US coast. Deep Seas Res. 24, 753–773.

Kideys, A.E., Kovalev, A.V., Shulman, G., Gordina, A., Bingel, F., 2000. A review of zooplankton investigations of the Black Sea over the last decade. J. Marine Syst. 24, 355–371.

Kovalev, A.V., Neirman, U., Melnikov, V.V., Belokopytov, V., Uysal, Z., Kideys, A.E., Unsal, M., Altukov, D., 1998. Long term changes in the Black Sea zooplankton: the role of natural and anthropogenic factors. In: Ivanov, L., Oguz, T. (Eds.), Ecosystem Modeling as a Management Tool for the Black Sea, vol. 1. Kluwer Academic Publishers, Dordrecht, pp. 221–234 NATO ASI Series 2, Environment-Vol. 47.

Kuhn, W., Radach, G., 1997. A one-dimensional physical-biological model study of the pelagic nitrogen cycling during the spring bloom in the Northern North Sea (FLEX'96). J. Mar. Res. 55, 687–734.

Lancelot, C., Hannon, E., Becquevort, S., Veth, C., de Baar, H.J.W., 2000. Modeling phytoplankton blooms and carbon export in the Southern Ocean: dominant controls by light and iron in the Atlantic sector in Austral spring 1992. Deep-Sea Res. I 47, 1621–1662.

Lebedeva, L.P., Shushkina, E.A., 1994. Modeling the effect of *Mnemiopsis* on the Black Sea plankton community. Oceanology 34, 72–80 English translation.

Levy, M., Memery, L., Andre, J.M., 1998. Simulation of primary production fluxes in the Northwestern Mediterranean Sea. J. Mar. Res. 56, 197–238.

McClain, C.R., Arrigo, S.R., Tai, K.S., Turk, D., 1996. Observations and simulations of physical and biological processes at OWS P 1951–1980. J. Geophys. Res. 101, 3697–3713.

McCreary, J.P., Kundu, P.K., Molinari, R.L., 1993. A numerical investigation of dynamics, thermodynamics and mixed-layer processes in the Indian Ocean. Progr. Oceanogr. 31, 181–244.

McCreary, J.P., Kohler, K.E., Hood, R.R., Olson, D.B., 1996. A four-component ecosystem model of biological activity in the Arabian Sea. Prog. Oceanogr. 37, 193–240.

Murray, J.W., Codispoti, L.A., Friederich, G.E., 1995. Oxidation–reduction environments: The suboxic zone in the Black Sea. In: Huang, C.P., O'Melia, C.R., Morgan, J.J. (Eds.), Aquatic chemistry: Interfacial and interspecies precosses, pp. 157–176 ACS Advances in Chemistry Series No. 224.

Mutlu, E., 1999. Distribution and abundance of ctenophores and their zooplankton food in the Black Sea. II. Mnemiopsis leidyi. Marine Biol. 135, 603–613.

Nezlin, N.P., Kostianoy, A.G., Gregoire, M., 1999. Patterns of seasonal and interannual and export changes of surface chlorophyll concentrations in the Black Sea revealed from the remote sense data. Remote Sens. Environ. 69, 43–55.

Niiler, P.P., Kraus, E.B., 1977. One dimensional models of the upper ocean. In: Kraus, E.B. (Ed.), Modelling and Prediction of the Upper Layers of the Ocean. Pergamon Press, New York, pp. 143–172.

Oguz, T., Salihoglu, B., 2000. Simulation of eddy-driven phytoplankton production in the Black Sea. Geophys. Res. Lett. 27 (14), 2125–2128.

Oguz, T., Ducklow, H.W., Malanotte-Rizzoli, P., Tugrul, S., Nezim, N., Unluata, U., 1996. Simulation of annual plankton productivity cycle in the Black Sea by a one-dimensional physical-biological model. J. Geophys. Res. 101, 16585–16599.

Oguz, T., Ducklow, H.W., Malanotte-Rizzoli, P., Murray, J.W., Vedernikov, V.1., Unluata, U., 1999. A physical-biochemical model of plankton productivity and nitrogen cycling in the Black Sea. Deep-Sea Res. I 46, 597–636.

Oguz, T., Ducklow, H.W., Malanotte-Rizzoli, P., 2000. Modeling distinct vertical biogeochemical structure of the Black Sea: Dynamical coupling of the Oxic, Suboxic and Anoxic layers. Global Biogeochem. Cycles 14, 1331–1352.

Oguz, T., Ducklow, H.W., Purcell, J.E., Malanotte-Rizzoli, P., 2001a. Modeling the response of top-down control exerted by gelatinous carnivores on the Black Sea pelagic food web. J. Geophys. Res. 106, 4543–4564.

Oguz, T., Murray, J.W., Callahan, A.E., 2001b. Modeling redox cycling across the suboxic-anoxic interface zone in the Black Sea. Deep-Sea Res. I 48, 761–787.

Oschlies, A., Garcon, V., 1999. An eddy-permitting coupled physical-biological model of the North Atlantic. 1. Sensitivity to advection numerics and mixed layer physics. Global Biogeochem. Cycles 13, 135–160.

Pace, M.L., Glasser, J.E., Pomeroy, L.R., 1984. A simulation analysis of continental shelf food webs. Marine Biol. 82, 47–63.

Radach, G., Moll, A., 1993. Estimation of the variability of production by simulating annual cycles of phytoplankton in the central North Sea. Prog. Oceanogr. 31, 339–419.

Rass, A.H., Gurney, W.S.C., Heath, M.R., Hay, S.J., Henderson, E.W., 1993. A strategic simulation model of a fjord ecosystem. Limnol. Oceanogr. 38, 128–153.

Sharpless, J., Tett, P., 1994. Modelling the effect of physical variability on the midwater chlorophyll maximum. J. Mar. Res. 52, 219–238.

Stramska, M., Dickey, T.D., 1993. Phytoplankton bloom and the vertical thermal structure of the upper ocean. J. Mar. Res. 51, 819–842.

Stramska, M., Dickey, T.D., 1994. Modelling phytoplankton dynamics in the northeast Atlantic during the initiation of the spring bloom. J. Geophys. Res. 52, 10241–10253.

Sverdrup, H.U., 1953. On conditions of the vernal blooming of phytoplankton. J. Cons. Explor. Mer. 18, 287–295.

Taylor, A.H., Stephens, J.A., 1993. Diurnal variations of convective mixing and the spring bloom of phytoplankton. Deep-Sea Res. II 40, 389–408.

Taylor, A.H., Harbour, D.S., Harris, R.P., Burkill, P.H., Edwards, E.S., 1993. Seasonal succession in the pelagic ecosystem of the North Atlantic and the utilization of nitrogen. J. Plank. Res. 15, 875–891.

Towsend, D.W., Keller, M.D., Sieracki, M.E., Ackleson, S.G., 1992. Spring phytoplankton blooms in the absence of vertical water column stratification. Nature 360, 59–62.

Varela, R., Cruzado, A., Tintore, J., Ladona, E., 1992. Modeling the deep-chlorophyll maximum: A coupled physical-biological approach. J. Mar. Res. 50, 309–315.

Vedernikov, V.1., Demidov, A.B., 1997. Vertical distributions of primary production and chlorophyll during different seasons in deep part of the Black Sea. Oceanology (English translation) 37, 376–384.

Vinogradov, M.E., Shushkina, E.A., Mikaelyan, A.S., Nezlin, N.P., 1999. Temporal (seasonal and interannual) changes in ecosystem of the open waters of the Black Sea. In: Besiktepe, S.T., Unluata, U., Bologa, A.S. (Eds.), Environmental degradation of the Black Sea: Challenges and Remedies. Kluwer Academic Publishers, Dordrecht, pp. 109–129 NATO ASI Series 2, Environmental Security-Vol. 56.

Yilmaz, A., Yunev, O.A., Vedernikov, V.I., Moncheva, S., Bologa, A.S., Cociasu, A., Ediger, D., 1998. Unusual temporal variations in the spatial distribution of chlorophyll-a in the Black Sea during 1990–1996. In: Ivanov, L., Oguz, T. (Eds.), Ecosystem Modeling as a Management Tool for the Black Sea, vol. 1. Kluwer Academic Publishers, Dordrecht, pp. 105–120 NATO ASI Series 2, Environment-Vol.47.

Zavaterelli, M., Baretta, J.W., Baretta-Bekker, J.G., Pinardi, N., 2000. The dynamics of the Adriatic Sea ecosystem. An idealized model study. Deep-Sea Res. I 47, 937–970.